EFFECT OF DEPOSITION TEMPERATURE ON OPTICAL PROPERTIES OF ALUMINUM OXIDE THIN FILMS PREPARED BY ATOMIC LAYER DEPOSITION

Liu Chundong[1], Xu Hailong[2], Shi Shuzheng[1,3,4], Wang Zhanying[1], Han Yifan[1], Pang Yongjun[1]*
[1] School of Mechanical Engineering, Architecture University of Hebei, Zhangjiakou; Hebei 075000;
[2]Test Center, China Coal Research Institute, Beijing 100013;
[3]HBIS Group Co., Ltd., Shijiazhuang; Hebei 050023;
[4]College of Metallurgy and Energy, North China University of Science and Technology, Tangshan; Hebei 063210.
Emails: shishuzheng2000@126.com

Abstract – Aluminium oxide (Al_2O_3) thin film has significant applications in optoelectronic devices due to its excellent photoelectric properties. To investigate the effect of deposition temperature on the photoelectric properties of ALD-Al_2O_3 films, samples with different deposition temperatures were prepared on silicon and K9 glass substrates using atomic layer deposition (ALD). The crystal structure and surface morphology of the samples were characterized using X-ray diffraction (XRD) and atomic force microscopy (AFM), respectively. The thickness, refractive index and extinction coefficient of the films were measured by spectroscopic ellipsometry (SE) in the wavelength range of 275~800 nm and fitted by Tauc-Lorentz (T-L) model. The fitted thickness and bandwidth results were verified using scanning electron microscopy (SEM) and ultraviolet-visible (UV-VIS) absorption spectroscopy. The results show that the surface of the ALD-Al_2O_3 film is smooth and dense at low temperatures. The surface roughness was approximately 0.3 nm, which was measured with AFM, and this value differs from the SE fitting results due to the local minimum obtained by SE, while the AFM test is a global minimum. The growth rate of 100cycles sample is about 0.1 nm/cycle, and the band gap is about 3.30 eV by SE. The 500cycles sample thickness is 54.9 nm measured by SEM, and the band gap is about 3.25 eV by UV-VIS extrapolation. The accuracy of the fitted model is verified by the correspondence between the fitted and test results.

Keywords: Aluminum oxide (Al_2O_3); Atomic layer deposition (ALD); Microstructure; Optical properties; Spectroscopic ellipsometry (SE).

1. Introduction

Aluminium oxide (Al_2O_3) is widely applied to the field of optics, batteries and microelectronics for its advantages of high dielectric constant, good stability, thermal conductivity and low refractive index [1-2]. The main preparation methods of Al_2O_3 thin films include chemical vapor deposition [3], electron beam evaporation [4], magnetron sputtering [5], pulse laser deposition [6]and atomic layer deposition [7], etc. Among them, atomic layer deposition (ALD) is a low-temperature atomic chemical vapor deposition technology, which has the advantages of uniformity, compactness, high controllability of composition and thickness at the monolayer or Ågstrom level. Additionally, it enables high shape preservation and large-area preparation of thin films. Therefore, ALD technology was used to prepare Al_2O_3 films extensively [8], especially the application in optical thin film coating [9], electronic devices [10], anti-corrosion coating [11], passivation layer on the surface of solar cells [12], antibacterial nanocoating [13], and so on. The complex and variable crystal structure of Al_2O_3 is mainly due to its strong Al-O bond and atomic spatial ordering. When the Al_2O_3 films is deposited at temperatures below 400°C, it forms an amorphous structure with a "short-range ordered and long-range disordered". The unique atomic structure arrangement of amorphous Al_2O_3 makes it valuable for optical applications, including optical lenses, optical windows, anti-reflection coatings, and optical waveguiding [14]. However, the complexity of the amorphous structure and its sensitivity to process conditions make it difficult to control and predict material properties, especially the effect of deposition temperature on film properties. Therefore, it is necessary to study the influence of deposition temperature on the photoelectric parameters of Al_2O_3 thin films to predict their photoelectric characteristics and improve their performance.

Spectroscopic ellipsometry (SE) technology is a highly accurate and non-destructive measurement method commonly used to determine the thickness,

refractive index, surface roughness, dielectric constant, and other photoelectric parameters of film samples [15]. SE uses the principle that the polarization state changes when the incident light is reflected or transmitted through the sample. As a result, it is highly sensitive to the interface morphology and optical constants of the sample surface, with a sensitivity that can reach sub-nanometer levels. It should be noted that SE is an indirect method and the physical information in the measured spectra is usually obtained by parametrizing the dielectric functions using appropriate dispersion models. At present, the commonly used dispersion models are Forouhi-Bloomer model [16], Tauc-Lorentz model [17] and Cauchy model [18], etc. The photoelectric parameters of the sample can be predicted by an appropriate model to fit the ellipsometry parameters. Based on above advantages, scholars have conducted extensive research on ALD oxide films using SE technology. In 2014, D. Saha et al. [19] grew TiO_2 films on Si substrates using the ALD process. The test results show that the samples exhibited varying structural and morphological characteristics depending on the substrate temperature. The SE data were fitted using Tauc-Lorentz model. At 200°C, the surface of the anatase film becomes significantly rougher during the transition from amorphous to crystalline phase, and the increase in dispersion energy is related to the increase in film density and coordination number. In 2015, Zhang et al. [20] used ALD to deposit Al_2O_3 films with thickness below 50nm on Si substrate. The refractive index of the Al_2O_3 film before and after annealing was calculated using the Cauchy model. The Studies have shown that the refractive index decreases with the increase of film thickness, and the trend of refractive index change is corrected after annealing. This phenomenon is believed to be caused by mechanical stress in the ALD-Al_2O_3 film. In 2022, Qu et al. [21] deposited ultrathin AlN films of different thicknesses on Si substrates by ALD, and fitted the SE parameters using Cauchy model. The study demonstrated that the index of refraction increased with the films thickness until it reached a stable point. Although SE measurements of oxide films have been reported, studies on the effect of deposition temperature on the properties of Al_2O_3 films are rare. Therefore, it is necessary to establish an accurate dispersion model, and the study of the structure and photoelectric characteristics of ALD-Al_2O_3 films by changing the deposition temperature is very important to improve the performance of optical devices.

In this paper, the effect of deposition temperatures (T_s) evolution on the optoelectronic characteristic of Al_2O_3 films prepared by ALD has been investigated. The Al_2O_3 films were deposited on Si substrate and K9 glass substrate by ALD method. The atomic configuration and surface morphology were characterized by X-ray diffraction (XRD) and atomic force microscopy (AFM). The amplitude Ψ and phase Δ of the samples were measured by spectroscopic ellipsometry (SE) in the spectral range of 300~800nm. The Tauc-Lorentz (T-L) dispersion model was used to fit the SE parameters, and the structural parameters and optical constants of the film were extracted. Meanwhile, the relationship between the properties and T_s of ALD-Al_2O_3 is discussed in detail. A combination of scanning electron microscopy (SEM) and ultraviolet-visible (UV-VIS) absorption spectroscopy revealed the effect of T_s on the growth rate and optical bandgap, supporting the calculated results of SE.

2. Experiments and Methods

2.1 Preparation of Film Samples

The Al_2O_3 samples were prepared on 4 inches N-type Si [100] (thickness of 500 μm and resistivity of 1–10 Ω·cm.) and K9 glass (area of 2×2 cm^2) by ALD (TFS-200, Beneq Qy, Finland), respectively. T_s was controlled in the range of 150°C~300°C with 50 °C intervals. The ALD is 100 cycles with trimethylaluminum (TMA-$Al(CH_3)_3$) and deionized water vapor (H_2O) as aluminum and oxygen precursors, respectively. During deposition, the precursor was stored in a stainless-steel bubbler and kept at ~20°C using a cooling water circulation facility. High purity nitrogen N_2 (99.999%) was used to purify the reaction chamber, and the N_2 flow rate was controlled at 300sccm by a flow controller with a pressure of 2.0Torr. TMA and H_2O were alternately entrained in the N_2 carrier gas by switching the cylinder. ALD relies on two complementary and self-limiting chemical reactions between alternating pulses. Within each pulse, the precursor adsorbed on the substrate surface reacts to form a Al_2O_3 thin film. Figure 1 shows schematic of one cycle of ALD-Al_2O_3 growth process. The growth cycle consisted of the following four steps: (1) TMA was injected as the first precursor pulse for 0.3s; (2) high-purity N_2 purge 3s; (3) H_2O was injected as the second precursor pulse for 0.3s; (4) High-purity N_2 was purged for 3s, and the total time of deposition cycle was 6.6s. The ALD-Al_2O_3 reaction equation is described as two half-cycle reactions.

1st half cycle:

$$Al(CH_3)_3 + \text{Surface-OH} \rightarrow \text{Surface-O-}Al(CH_3)_2 + CH_4 \quad (1)$$

2nd half cycle:

$$\text{Surface-O-Al-}(CH_3)_2 + 2H_2O \rightarrow \text{Surface-O-Al-OH} + 2CH_4 \quad (2)$$

The overall cycle reaction:

$$2Al(CH_3)_3 + 3H_2O \rightarrow Al_2O_3 + 6CH_4 \quad (3)$$

The ALD-Al_2O_3 thin film can be deposited with single atomic layer accuracy by repeating the surface

chemical reactions with the (1)-(2)-(1)-(2) sequence, where the 1st half cycle plus 2nd half cycle is one ALD cycle. The thickness of the ALD-Al_2O_3 thin film can be precisely controlled by the number of ALD cycles. Compared with other technologies, ALD is more suitable for growing semiconductor thin film materials under low temperature conditions due to the high reaction activity of the precursor [22].

The advantages of ALD are as follows: precise thickness control with one monolayer precision, high conformality and good step coverage, excellent uniformity leading to large-area and large-batch capacity, accurate composition control, and in-situ atomic layer doping capability, low defect density, and good reproducibility [23, 24].

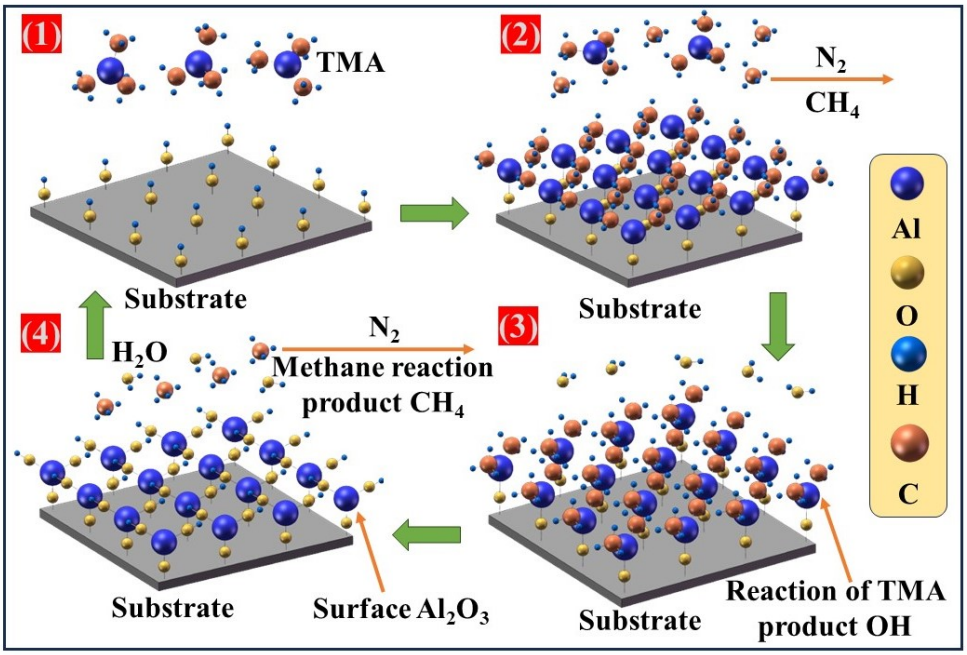

Figure 1: Schematic of one cycle of ALD-Al_2O_3 growth process.

2.2 Characterization and Testing

The crystal structures of the films were determined by X-ray diffractometer XRD (X 'Pert PRO, PANalytical B.V., The Netherlands) with scanning angles ranging 2θ=0°~80°. Atomic force microscopy AFM (VT-1000, Bruker Dimension Icon, Germany) was used to characterize the surface morphology of the film with a scanning range of 3μm×3μm. In particular, AFM chooses the tapping mode of the tip of the Si cantilever with a curvature radius of ~20nm, a spring constant of 5.5N/m, and a resonance frequency of ~180kHz. The optical transmittance of the films was measured using a UV-VIS spectrophotometer (UV-1700, SHIMADZU, Japan) in the wavelength range of 300~900nm, and the samples were grown on K9 glass. Spectroscopic ellipsometry (SE850, SENTECH, Germany) was employed to collect the ellipsometry parameters (Ψ, Δ) over the wavelength of 275~800 nm at an incidence angle of 65°.

2.3 Spectroscopic Ellipsometry Model

When light waves reflect or transmit on a film sample, their polarization states change, and the wave vectors are decomposed into the two components differ significantly *p*-polarization and *s*-polarization. Based on the differences in the ellipsometry parameters and their sensitivity to the sample surface topography, the optical parameters of the film can be obtained by fitting the ellipsometry measurements using the Fresnel equation [25], such as surface roughness, the refractive index (n) and the extinction coefficient (k) and dielectric function (ε), etc. Therefore, the measured values of the ellipsometry parameters (Ψ, Δ) at different wavelengths can be used to obtain the ellipsometry spectra of the thin film. Under the reflection measurement condition, the reflection coefficient (ρ) is defined as follows equation [26]:

$$\rho = \frac{R_p}{R_s} = \tan(\psi)\exp(\mathrm{i}\Delta) \tag{4}$$

Where, R_p and R_s are the Fresnel reflection coefficients of the p and s polarization components, respectively. tan (Ψ) is the amplitude ratio in polar coordinates, where Ψ ranges from 0 to π/2, and Δ is the phase difference, ranging from 0 to 2π.

The dielectric function (ε) is a critical electronic response function that reflects the interaction between the applied field and electrons in materials,

and indicates the degree of thin film medium response to spectral photon energy. From the measured Ψ and Δ, ε can be obtained from the following equation [27].

$$\varepsilon = \varepsilon_1 + i\varepsilon_2 = \varepsilon_0 \sin^2\phi_0 \left[1 + \tan^2\phi_0 \left(\frac{1-\rho}{1+\rho}\right)^2\right] \quad (5)$$

Where, ε_1 and ε_2 are the real and imaginary parts of the dielectric function, respectively. ε_0 is the vacuum dielectric function. ϕ_0 is the incidence angle.

There are two strategies for ellipsometry analysis. The first is the wavelength method, which is independent of the dispersion model of the material. The disadvantage of this method is that the optical constants obtained may be discontinuous and the measured film thickness is not accurate enough. Another method to overcome this shortcoming is spectral ellipticity, and the precondition for using this method is to establish an appropriate optical dispersion model. Therefore, considering the interband absorption, the single oscillator Tauc-Lorentz (T-L) dispersion relation is used to characterize the dielectric function of the material. In 1966, Jellison and Modine [28, 29] combined Tauc band-edge theory and Lorentz oscillator model to establish the T-L model, which can more accurately extract the optical constants between the conduction band and valence band of semiconductor materials, and solve the problem that the absorption of light waves below the band gap energy of semiconductors, resulting in the extinction coefficient not being zero. ε_2(E) is the product of the Tauc function and the Lorentz oscillator function as follows:

$$\varepsilon_2(E) = \begin{cases} \dfrac{ACEE_0}{\left(E^2 - E_0^2\right)^2 + C^2E^2} \dfrac{\left(E - E_g\right)^2}{E^2} & for\ \ E > E_g \\ 0 & for\ \ E \le E_g \end{cases} \quad (6)$$

Where, A is the amplitude factor of the Tauc-Lorentz oscillator, which is proportional to the density of the material and the elements of the momentum matrix. C is the spectral amplification factor, E_0 is the peak transition energy, and E_g is the band gap of the thin film material.

The real part ε_1(E) can be obtained using the Kramers-Kronig relation [30] as follows:

$$\varepsilon_1(E) = \varepsilon_1(\infty) + \frac{2}{\pi} P \int_{E_g}^{\infty} \frac{\tau\varepsilon_2(\tau)}{\tau^2 - E^2} d\tau \quad (7)$$

Where, $\varepsilon_1(\infty)$ is the dielectric function when the oscillator energy $E \to \infty$, and P is the Cauchy principal value. In the T-L model, the dielectric function of the film material is determined by five parameters A, C, E_0, E_g, $\varepsilon_1(\infty)$.

The scattering caused by the surface roughness of the thin film material will lead to optical depolarization, and a reasonable optical model is conducive to ellipsometry measurement.

Therefore, it is necessary to establish a physically feasible optical parameterized model to assign optical dispersion laws to each layer, and to obtain accurate Ψ and Δ curves in the iterative process by optimizing the model parameters. Figure 2 shows the optical model of Al_2O_3 thin film. The structure is divided into four layers from bottom to top: (1) Si substrate; (2) In the transition layer between Si and Al_2O_3 film, there is no high-energy ion bombardment in the ALD preparation process, and no penetration between materials, so the effect of the transition layer on the overall analysis can be ignored. (3) Al_2O_3 compact layer; (4) The surface rough layer of rough surface particles and air, and the pores and dense layers are evenly distributed in the surface rough layer. The Bruggeman effective medium approximation (EMA) theory [31] considers the physical roughness as a planar layer, which is optically represented as the volume weighted average of the film material and the pores. Therefore, the surface roughness layer is defined as a mixture of 50% Al_2O_3 bulk layer and 50% voids using EMA.

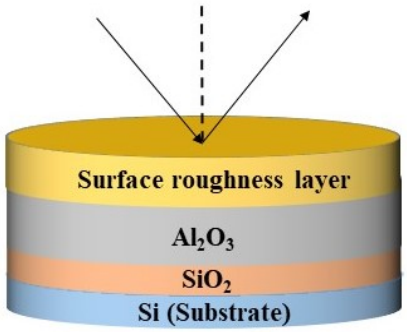

Figure 2: Optical model of spectroscopic ellipsometer

In the process of SE fitting, the objective optimization iterative function is used to find the optimal fitting solution, and the deviation degree between the fitted value and the measured value is evaluated by the root mean square error (MSE) function in equation (8) [30]. A smaller MSE value indicates a smaller prediction error of the dispersion model, and vice versa since.

$$\mathrm{MSE}^2 = \frac{1}{N-P} \sum_i \left[\left(\frac{\Psi_i^{cal} - \Psi_i^{exp}}{\sigma_i^{\Psi}} \right)^2 + \left(\frac{\Delta_i^{cal} - \Delta_i^{exp}}{\sigma_i^{\Delta}} \right)^2 \right] \quad (8)$$

Where, N and P are the total number of data points and the number of fitted model parameters, respectively. Ψ_i^{cal} and Δ_i^{cal} are the theoretical values fitted by the dispersion model, respectively. Ψ_i^{exp} and Δ_i^{exp} are the ellipsometry measurements, σ_i^{Ψ} and σ_i^{Δ}

are the standard deviations of Ψ and Δ, respectively. The best fit is achieved when the MSE value reaches the global minimum.

3. Results and Discussions

XRD is an effective method for analyzing the crystal structure of materials, as it is sensitive to the order of lattice arrangement in thin film materials.

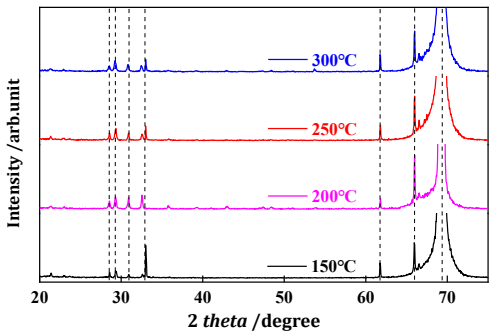

Figure 3 XRD spectra of Al_2O_3 thin film samples with different deposition temperatures

Figure 3 shows the XRD spectra of Al_2O_3 films prepared at different deposition temperatures (T_s). By comparing PDF#: 97-006-7788, It can be found that all samples have Si (400) super diffraction peak at 69.71°, and by comparing PDF#: 97-007-9637, it was found that the SiO_2 diffraction peak appears at 61.84° and 66.97°. It is because that a layer of about 100nm natural oxide layer on the Si substrate, and the Al_2O_3 film thickness is nanometer level prepared by the ALD process. Actually, the XRD ray penetration depth reaches several microns. Consequently, X-rays can penetrate the Al_2O_3 film and measure the diffraction peaks of Si and SiO_2. In addition, there are some amorphous diffraction packets between 25°~35°. Based on the characteristics of a low temperature ALD process and numerous flat noise peaks, it can be inferred that the ALD-Al_2O_3 film samples have poor crystallization and are mainly amorphous.

The roughness surface of the Al_2O_3 film will lead to large surface scattering and optical loss, and the surface flatness greatly affects the photoelectric characteristics of the film. In our study, AFM was used to characterize the surface morphology of the film samples, and NanoScope software was employed to calculate the root mean square roughness R_q.

$$R_q = \sqrt{\frac{\sum_{j=1}^{N} Z_j^2}{N}} \tag{9}$$

Where, Z_j is the surface height and N is the number of measurement points.

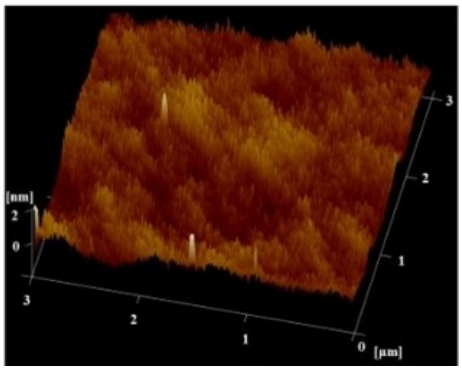

(a) T_s=150℃, R_q=0.362nm

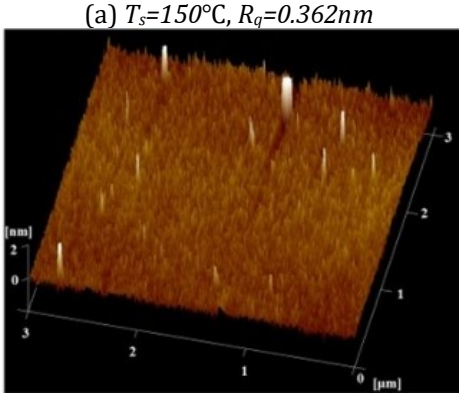

(b)T_s=200℃, R_q=0.299nm

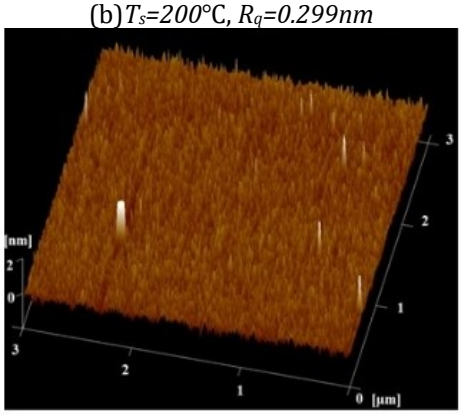

(c)T_s=250℃, R_q=0.244nm

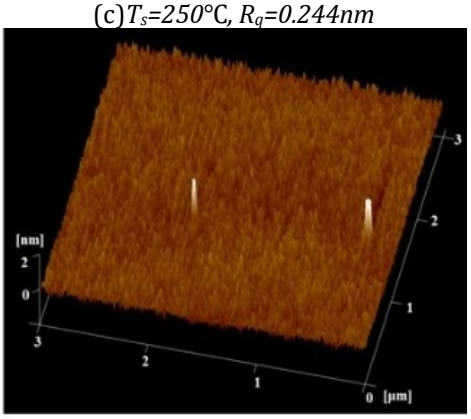

(d)T_s=300℃, R_q=0.212nm

Figure 4. 3D AFM images of Al_2O_3 thin film samples with different deposition temperatures

The 3D AFM morphology of the AlD-Al_2O_3film samples with different deposition temperatures, as shown in Figure 4. It can be seen that the surface of

the samples is smooth and crack-free, and shows an obvious change trend. R_q decreases from 0.362nm to 0.212nm with the increase of T_s from 150℃ to 300℃, which implies the surface quality of thin film can be improved through increasing the T_s. The test results can be considered that the AlD-Al_2O_3 film samples has a good surface flatness, and a smooth surface can improve the accuracy of SE measurement.

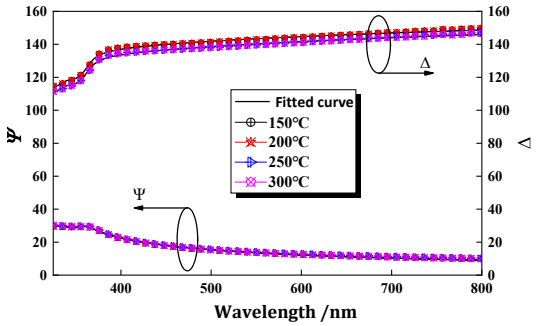

Figure 5 Ellipsometry spectra of Al_2O_3 thin film samples fitted by the T-L model with different deposition temperatures

Based on spectroscopic ellipsometry principle, the ALD-Al_2O_3 film samples deposited under different temperature conditions were measured by SE, and the T-L model was used for fitting analysis. Figure 5 shows the Al_2O_3 *thin film* samples ellipsometry spectra relationship between the measured and fitted by the T-L model with different deposition temperatures. The fitting results show that the curve characteristics are all below 400nm, and the measurement wavelength range is from 325 to 800nm, the shortest wavelength used in this paper is 275nm, which ensures the accuracy of the fitting. Throughout the UV-VIS ible region, the T-L model provides a good fit to the ellipticity spectrum of Al_2O_3 thin film samples. The MSE of the spectrum line at low-temperature is 0.76, and the high-temperature segment is 0.57. The experimental data are in good agreement with the fitting results. The MSE of all samples is less than 1, indicating high credibility of the ellipticity parameters extracted by the T-L model.

Table 1 Electronic and structural parameters extracted from SE analysis based on the T-L model of 100 cycles ALD-Al_2O_3 thin film samples with different deposition temperatures

T_s / ℃	150	200	250	300
$\varepsilon_1(\infty)$	2.36	2.90	2.71	2.86
A	453.85	21.44	44.51	399.46
C	750.39	369.93	322.07	799.99
E_0 /eV	15.06	22.86	25.68	3.51
E_g /eV	3.39	3.30	3.31	3.31
d_s /nm	0.83	0.79	0.70	0.63
d /nm	11.13	10.98	11.16	10.96
MSE	0.76	0.76	0.58	0.57

Table 1 summarizes the T-L model parameters obtained from the regression analysis for the samples deposited with different deposition temperatures. It can be seen that the thickness d of AlD-Al_2O_3 film samples deposited for 100 cycles at different temperatures is basically the same, stabilizing at a relatively stable interval between 10.96nm to 11.16nm, and the corresponding growth rate is ~0.11nm/cycle. To verify the accuracy of the film thickness results extracted by the T-L model, 500 cycles ALD-Al_2O_3 film sample was deposited at 200°C and the thickness is 53.65nm, which was measured by SEM as shown in Figure 6.

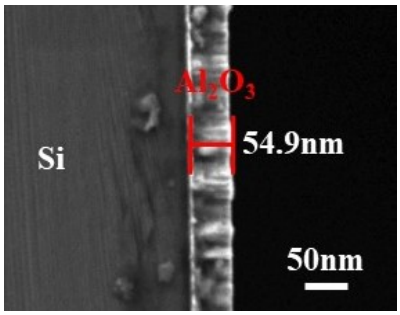

Figure 6 SEM cross section of 500 cycles ALD-Al_2O_3 thin film sample

Based on the AlD-Al_2O_3 film samples thickness of 100 cycles at the same temperature in Table 1, it can be deduced that the thickness of the AlD-Al_2O_3 film sample with 500 cycles is approximately 54.9nm. This indicates that the thickness parameters extracted are reliable by SE. However, there is a thickness difference of approximately 1.25nm between the results obtained from the two testing methods. The main reasons for the discrepancies can be attributed to several factors. (1) the growth rate of each cycle of ALD is not constant. (2) the SE analysis used to calculate thickness has an error of approximately 0.5nm. (3) the two thickness measurement methods of SE and SEM have different principles, resulting in internal differences. (4) SE is an indirect measurement method, and the obtained result may be a local minimum rather than a global minimum, resulting in a certain degree of calculation error. According to the ellipsometry measurement principle, the true thickness of the film d as follows:

$$d = f(n, d_1) = md_{01} + d_1 = \frac{m\lambda}{\sqrt{n^2 - n_1^2 \sin^2 \phi_1}} + d_1 \quad (10)$$

Where, n is refractive index measurement of the film. m and d_{01} are the cycle number and cycle thickness of the true thickness, respectively. n_1 is the refractive index of the surface rough layer at the corresponding wavelength points, respectively. λ and d_1 are the wavelength of the light wave and the thickness value in one cycle, respectively. ϕ_1 is the refraction angle of the incident beam after refraction

through the surface rough layer, which is the incidence angle of the film body layer. It can be seen from Eq. (10) that the calculated thickness of the film is strongly influenced by the material properties and the refractive index of the rough surface layer during the data fitting process.

Based on the roughness data presented in Table 1 and Figure 4, there is a difference of approximately 0.4nm between the ellipsometry fitting value d_s and the AFM test value d_{rms}. However, the trend of the two values remains consistent as the roughness decreases with increasing temperature. In 1996, J. Koh et al. [32] established an empirical relationship between the film roughness d_s and d_{rms} obtained by SE and AFM, d_s=1.48drms+0.428nm. When substituting d_{rms} =0.299nm at 200°C into the above relationship, we obtain d_s =0.872nm. There is a difference between the obtained result and the fitting result. However, it cannot be fully explained that the d_s extracted by the T-L model is not accurate enough. J. Koh et al. studied α-Si_xC_{1-x}···H films, and the empirical formula may not apply to ALD-Al_2O_3 films. The difference in roughness is primarily due to the discrepancy in scanning range between the elliptical measurement instrument, which has a laser spot size in the order of millimetres, and the AFM measurement, which has a scanning range in the order of micrometre. This difference in scanning range is likely to cause a deviation in the test results.

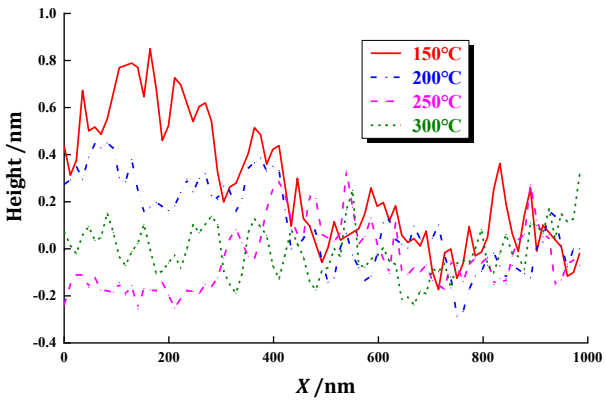

Figure 7 Height profile curve of Al_2O_3 thin film samples with different deposition temperatures

A height profile curve with a length of 1000 nm was taken at random on the film sample surface, as shown in Figure 7. It can be seen that with the increase of T_s, the surface undulation of the sample has a clear decreasing trend, which is basically consistent with the AFM measurement results. Therefore, it is necessary to apply a transition layer on the surface of the film to reflect the rough layer formed by particles and air on the surface of the ALD-Al_2O_3 film. Since the thickness of the rough layer is on the order of sub-nanometer, and the total thickness of the film is estimated to be about ten nm, the proportion of the rough layer has a certain influence on the overall fitting results of the film. In addition, Eq. (10) shows that the rough layer should also depend on its own refractive index, while the porosity has been set to 50% in the optical model of Figure 1. Therefore, the refractive index of the rough layer mainly depends on the refractive index of the bulk layer of the Al_2O_3 film.

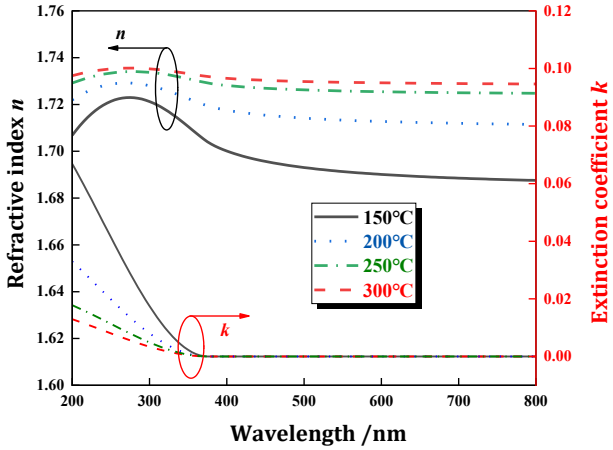

Figure 8 Refractive index and extinction coefficient of Al_2O_3 thin films with different deposition temperatures

The n/k value curves of AlD-Al_2O_3 film samples with different T_s were extracted using the parameters listed in Table 1, as shown in Figure 8. The relationship between the n/k value of the film sample and T_s is apparent, with both values changing in opposite trends. The film samples that have the highest n value and the lowest k value are those with T_s=300°C. At a wavelength of 370nm, n increases from 1.704 to 1.733 with increasing T_s. The k curve displays an inflection point at a wavelength of approximately 370nm (equivalent to 3.3eV) due to the band-edge absorption of Al_2O_3, indicating the onset of photon absorption. The n-curve exhibits strong dispersive properties and reaches a maximum near 300nm, which originates from the interband transitions of electrons in the film. Meanwhile, the interfacial layer also affects the n/k value of the sample. This impact may be due to surface defects, such as stress-strain or imperfect crystallization, which are determined by the number of activated groups and saturated adsorption capacity. The AlD-Al_2O_3 film samples with higher T_s may exhibit stress-strain, and amorphous phases may appear at low temperatures. As T_s increases, defects may decrease, and the trend of n/k values is similar to that of the Al_2O_3 bulk layer. However, due to the existence of the interface layer, the influence is inevitable. These results indicate that T_s plays an important role in the optical properties of ALD-Al_2O_3 films. Therefore, part of the difference between the above film thickness, as well as the thickness of the rough layer, may come from the difference in n values. This also verifies the change of the energy band gap with T_s previously obtained by SE.

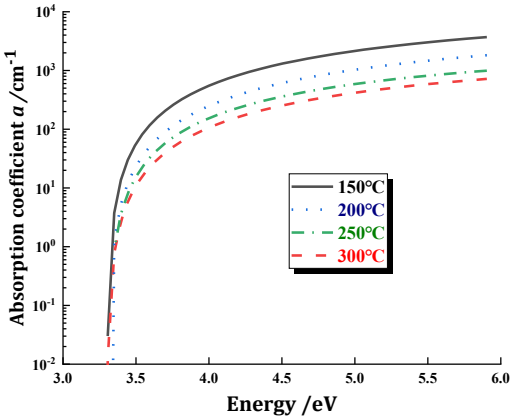

Figure 9 Absorption coefficient α of Al_2O_3 thin films with different deposition temperatures

Figure 9 shows the absorption coefficient α of the Al_2O_3 film sample with different deposition temperatures. It is evident that α sharply increases in the energy range of 3.0 to 3.5eV, covering a range of four orders of magnitude. Based on the summation rule in the dielectric function [33], it is due to the increase in effective valence electrons per unit volume of the material. In the energy region above ~3.3eV, α decreases with the increase of T_s, while the change trend is opposite below ~3.3eV. The reason for this result is that AlD-Al_2O_3 film samples deposited at low temperatures have fewer band-tailed states and a smaller optical band-gap E_g. In all samples, the difference is mainly observed in the energy range above ~3.3eV, indicating that the film absorptive capacity depends on the number of its band tails.

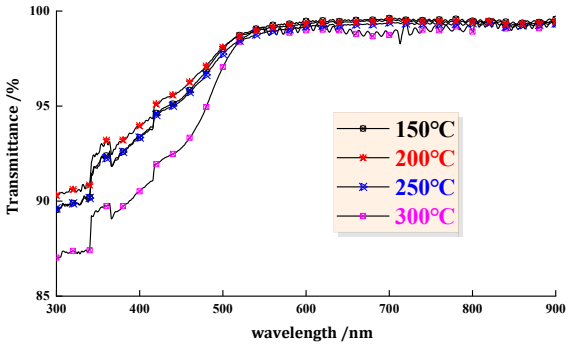

Figure 10 Optical transmittance spectra with different deposition temperatures by UV-VIS transmittance measurement.

To verify the E_g results of the SE extraction of ALD-Al_2O_3 samples, the UV-VIS transmission spectra in the wavelength range from 300 to 900nm were examined as shown in Figure 10. The transmittance curve shows that the sample maintains a transmittance between 98.78% and 99.44%. As the deposition temperature rises, the transmittance of the fabricated ALD-Al_2O_3 samples increases across the entire wavelength range examined.

This improvement is primarily attributed to two factors: higher deposition temperatures promote increased film density, thereby minimizing scattering losses during light propagation; and they also enhance the film crystallinity, reducing inherent absorption losses. In the far-infrared region (400nm), all samples exhibit transmittance approaching 100%, indicating that light within this wavelength range can traverse the ALD-Al_2O_3 samples almost unimpeded. However, in the near-infrared and visible regions, transmittance gradually decreases as the wavelength shortens, which is closely tied to the intrinsic wide bandgap structure and electronic transition levels of the ALD-Al_2O_3 material itself. Notably, the sample deposited at 300°C displays a pronounced transmittance dip in the mid-infrared range (300~400nm), corresponding to a characteristic absorption peak of the ALD-Al_2O_3 samples. This phenomenon suggests that a certain concentration of defects or impurities exists in thin films prepared at higher temperatures, leading to the absorption of photons in the corresponding wavelength range by these introduced defect levels. Consequently, while increasing the deposition temperature to achieve superior crystallinity, it is crucial to regulate the introduction of defects and impurities to avoid adverse effects on transmittance within specific wavelength bands [34].

Additionally, multiple step-like transitions are observed in the long-wavelength direction of the UV-VIS transmittance spectra. These transitions commonly occur when the thickness of the alumina film approaches or exceeds a critical wavelength. The occurrence of these transitions can be attributed to two main factors: Firstly, due to the intrinsic optical properties and material parameters of alumina, it exhibits step-like transmittance transitions within a specific range of several hundred to several thousand nanometers, with different wavelength ranges corresponding to different numbers of multiple step-like transitions. Secondly, the number of step-like transitions depends on the relationship between the film thickness and the incident light wavelength. Multiple step-like transitions are commonly observed when the film thickness is close to or exceeds half the wavelength of light [35].

The absorption coefficient α can be calculated by UV-VIS, and the optical band gap E_{Tauc} can be plotted using extrapolation method. The Tauc Equation [28] can be expressed as follows.

$$\alpha = \frac{4\pi K}{\lambda} = \frac{K\left(E - E_{Tuac}\right)^n}{E} \tag{13}$$

Where, k and λ are the extinction coefficient and incident wavelength, respectively. K is a constant and E is the photon energy. n=2 for the indirect

electron transition and n=1/2 for the direct transition. As the ALD-Al_2O_3 sample is an amorphous film with an indirect band gap, we take n=2.

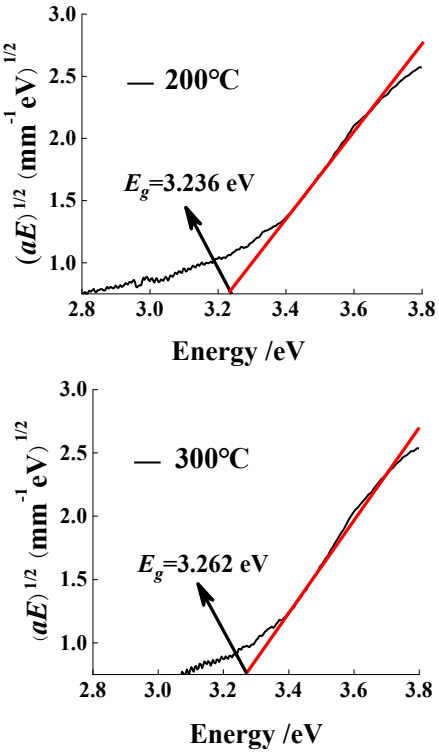

Figure 11 The optical band gaps from the plots of $(\alpha E)^{1/2}$ vs. E_{Tauc} of 200°C and 300°C using the Tauc extrapolation method.

Based on Tauc theory, the linear characteristic of the Tauc curve is a direct result of the parabolic distribution of electron energy. Therefore, the band gap of the ALD-Al_2O_3 film can be determined using the linear extrapolation of the absorption coefficient α and the Tauc mapping method. The steep linear part of the absorption edge is extrapolated to αE=0, and the corresponding band gap width E_{Tauc} is determined by finding the intersection with the X-axis. The E_{Tauc} values were determined using Tauc mapping method at 200°C and 300°C, as illustrated in Figure 11. It is evident that the E_{Tauc} remained approximately at 3.2eV, with a corresponding slope close to zero, and the curve did not exhibit significant fluctuations. The E_g and E_{Tauc} results (~3.3eV) were consistent, which further confirms the reliability of the SE results. However, there are some differences between E_g and E_{Tauc}, which may be due to the following three main reasons: (1) The Tauc model introduces the localization of the electron wavefunction and subband-gap absorption in the gap band. However, in the T-L model, when E is equal to E_{TL}, the value of $\varepsilon(E)$ is forced to be zero, resulting in a photoelectron transition below the band gap of zero. (2) UV-VIS measurements only record transmittance and ignore polarization information. (3) The Tauc extrapolation method involves a human-controlled fit, which can vary from person to person and is a major factor in the bias of E_g and E_{Tauc} results.

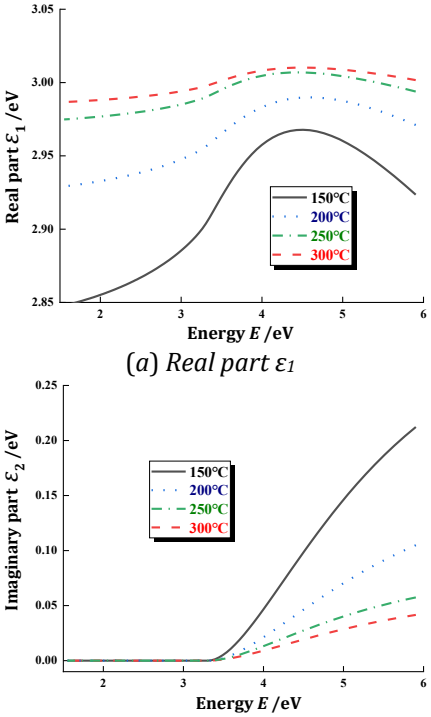

(*a*) *Real part* ε_1

(*b*) *Imaginary part* ε_2

Figure 12 Dielectric functions of Al_2O_3 thin films with different deposition temperatures, real part ε_1 (a), imaginary part ε_2 (b).

The dielectric function ε reflects the interaction between the electrons and the external field in the material, which determines the dielectric response characteristics of the thin film material. Figure 12 shows the dielectric function of the Al_2O_3 film sample, which includes (a) the real part ε_1 and (b) the imaginary part ε_2. As can be seen from the figure, all curves exhibit a systematic change with T_s increases. In Figure12(b) ε_2 spectrum, the absorption peak appears at E≈3.3eV, and the arrangement of disordered atoms in the amorphous phase does not have translational symmetry. It follows from $\varepsilon_2=n_2 \cdot k_2$ that $\varepsilon_2 \to 0$ in the T-L model as $E \to \infty$. For all Al_2O_3 film samples, when the photon energy is in the range of 0~3.3eV, ε_2=0, this is because the T-L model prohibits the electronic transition smaller than the band-gap E_{TL} fitted by the model [36]. The absorption of the Al_2O_3 thin films is indicated by the curve after the non-zero point, with the boundary point between zero and non-zero values representing the optical band-gap.

4. Conclusions

In this paper, aluminium oxide (Al_2O_3) thin films prepared on Si substrate and K9 glass by varying the deposition temperature using ALD technology. XRD

and AFM test results show that the film samples are dominated by amorphous structure with good surface flatness, and the R_q value decreases with the increase of T_s. The T-L model was established based on the characteristics of ALD-Al_2O_3 film, and the ellipsometry parameters of the samples were fitted to analysed their photoelectric characteristics. The results show that the thickness of ALD-Al_2O_3 films deposited at different temperatures for 100 cycles is almost the same, and the corresponding growth rate is ~0.11nm/cycle. The roughness of ALD-Al_2O_3 films measured is approximately 0.3nm by AFM, which shows a discrepancy with the SE fitting results. This difference is mainly due to the local minimum obtained by SE, while the AFM test provides a global minimum. The band gap E_g of SE fitting sample is ~3.30eV by T-L model, and E_{Tauc} obtained by UV-VIS extrapolation is ~3.25eV. The degree of agreement between the fitting results and the test results verifies the accuracy of the fitting model. The ALD-Al_2O_3 preparation method is simple and feasible, and the film exhibits excellent photoelectric properties. The parameters extracted by the fitting model are consistent with reality. This method can be applied to the preparation and analysis of the metal-oxide-semiconductor films.

Acknowledgement

This work is supported by The Doctoral Research Start-up of Hebei University of Architecture [grant number: B-202301]; Basic Scientific Research Business Project of Colleges and Universities in Hebei Province [grant number: 2022QNJS01]; Zhangjiakou City key research and development plan special [grant number: 2311022B].

References

[1] Mavric A, Valant M, Cui C, et al. Advanced applications of amorphous alumina: From nano to bulk[J]. Journal of Non-Crystalline Solids. 2019, 521:119493. doi: https:// 10.1016/j.jnoncrysol.2019.119493.

[2] Spencer J A, Mock A L, Jacobs A G, et al. A review of band structure and material properties of transparent conducting and semiconducting oxides: Ga_2O_3, Al_2O_3, In_2O_3, ZnO, SnO_2, CdO, NiO, CuO, and Sc_2O_3 [J]. Applied Physics Reviews. 2022, 9, 1:011015. doi: https:// 10.1063/5.0078037.

[3] Yang K, Zhong S, Zhou XM, et al. Controllable Al_2O_3 coating makes TiO_2 photocatalysts active under visible light by pulsed chemical vapor deposition [J]. Chemical Engineering Science. 2023, 86:2129-35. doi: https:// 10.1016/j.ces.2023.118792.

[4] Lan Y, Zou Y, Ma X, et al. Fabrication of amorphous Al_2O_3 optical film with various refractive index and low surface roughness[J]. Materials Research Express, 2020, 7(8):086405. doi: https:// 10.1088/2053-1591/abb0af.

[5] Noikaew B, Wangmooklang L, Niyomsoan S, et al. Preparation of transparent alumina thin films deposited by RF magnetron sputtering[J]. Journal of Metals Materials and Minerals. 2021, 31(2):96–103. doi: https:// 10.14456/jmmm.2021.25.

[6] Manica D, Ion V, Sopronyi M, et al. Mechanical properties characterization for thin layers oxide (Al_2O_3), deposited by PLD-large area[J]. Applied Physics A-Materials Science & Processing. 2022, 128, 11:983. doi: https:// 10.1007/s00339-022-06098-4.

[7] Zaidi SJA, Park JC, Han JW. Interfaces in Atomic Layer Deposited Films: Opportunities and Challenges[J]. Small Science, 2023, 3(10): 111-131. doi: https:// 10.1002/smsc.202370019.

[8] Leskelä M, Mattinen M, Ritala M. Review Article: Atomic layer deposition of optoelectronic materials[J]. Journal of Vacuum Science & Technology B, 2019, 37(3):030801. doi: https:// 10.1116/1.5083692.

[9] Paul P, Pfeiffer K, Szeghalmi A. Antireflection Coating on PMMA Substrates by Atomic Layer Deposition[J]. Coatings, 2022, 10(1):64. doi: https:// 10.3390/coatings10010064.

[10] Wang G, Duan Y. Efforts of implementing ultra-flexible thin-film encapsulation for optoelectronic devices based on atomic layer deposition technology[J]. Smartmat, 2024, Early Access. doi: https:// 10.1002/smm2.1286.

[11] Xu FM, Luo L, Xiong L, et al. Microstructure and corrosion behavior of ALD Al2O3 film on AZ31 magnesium alloy with different surface roughness[J]. Journal of Magnesium and Alloys, 2020, 8(2):480-492. doi: https:// 10.1016/j.jma.2019.06.003.

[12] Suh D. Status of Al2O3/TiO2-Based Antireflection and Surface Passivation for Silicon Solar Cells[J]. Physica Status Solidi-Rapid Research Letters, 2021, 15(10):2100236. doi: https://10.1002/pssr.202100236.`

[13] Nazarov D, Kozlova L, Rogacheva E, et al. Atomic Layer Deposition of Antibacterial Nanocoatings: A Review[J]. Antibiotics-Basel, 2023, 12(12):1656. doi: https://10.3390/antibiotics12121656.

[14] Khanna A, Bhat D G, Harris A, et al. Structure-property correlations in aluminum oxide thin films grown by reactive AC magnetron sputtering[J]. Surface and Coatings Technology, 2006, 201(3-4):1109-1116. doi: https:// 10.1016/j.surfcoat.2006.01.033.

[15] Joo KN and Park H. Recent Progress on Optical Tomographic Technology for Measurements and Inspections of Film Structures[J]. Micromachines, 2022, 13, 7:1074. doi: https:// 10.3390/mi13071074.

[16] Forouhi A R, Bloomer I. Optical dispersion relations for amorphous semiconductors and amorphous dielectrics[J]. Physical review B, 1986, 34(10): 7018-7026. doi: https:// 10.1103/PhysRevB.34.7018.

[17] Jellison Jr G E, Modine F A. Parameterization of the optical functions of amorphous materials in the interband region[J]. Applied Physics Letters, 1996, 69(3): 371-373. doi: https:// 10.1063/1.118064.

[18] Fujiwara H. Spectroscopic ellipsometry: principles and applications. Chichester: John Wiley & Sons; 2007, PP 170.

[19] Saha D, Ajimsha R S, Rajiv K, et al. Spectroscopic ellipsometry characterization of amorphous and crystalline TiO_2 thin films grown by atomic layer deposition at different temperatures[J]. Applied Surface Science, 2014, 315:116-123. doi: https:// 10.1016/j.apsusc.2014.07.098.

[20] Wang ZY, Zhang RJ, Lu HL, et al. The impact of thickness and thermal annealing on refractive index for aluminum oxide thin films deposited by atomic layer deposition[J]. Nanoscale Research Letters, 2015, 10:46. doi: https:// 10.1186/s11671-015-0757-y.

[21] Minni Q, Liying W, Xueqian D, et al. Ellipsometry Characterization of Ultrathin AlN Film Grown by Atomic Layer Deposition [J]. Micronanoelectronic Technology, 2022(002):059. doi: https:// 10.13250/j.cnki.wndz.2022.02.010.

[22] Kim H M, Kim D G, Kim Y S, et al. Atomic layer deposition for nanoscale oxide semiconductor thin film transistors: review and outlook[J]. International Journal of Extreme Manufacturing, 2023, 5(1):012006-012006. doi: https:// 10.1088/2631-7990/acb46d.

[23] Johnson R W, Hultqvist A, Bent S F. A brief review of atomic layer deposition: from fundamentals to applications[J]. Materials today, 2014, 17(5): 236-246. doi: https:// 10.1016/j.mattod.2014.04.026

[24] Yasmeen S, Ryu S W, Lee S H, et al. Atomic layer deposition beyond thin film deposition technology[J]. Advanced Materials Technologies, 2023, 8(20): 2200876. doi: https:// 10.1002/admt.202200876

[25] Jellison G E. Handbook of Ellipsometry[M]. Elsevier Inc., 2005, PP 73-76.

[26] Fujiwara H. Spectroscopic Ellipsometry: Principles and Applications[M]. John Wiley & Sons Ltd, 2007, PP 81-84.

[27] Hilfiker J N, Singh N, Tiwald T, et al. Survey of methods to characterize thin absorbing films with Spectroscopic Ellipsometry[J]. Thin Solid Films, 2008, 516(22), 7979-7989. doi: https:// 10.1016/j.tsf.2008.04.060.

[28] Tauc J, Grigorovici R, Vancu A. Optical properties and electronic structure of amorphous germanium[J]. Physica Status Solidi, 1966, 15(2): 627-637. doi: https:// 10.1002/pssb.19660150224

[29] Jellison G E and Modine F A. Parameterization of the optical functions of amorphous materials in the interband region[J]. Applied Physics Letters, 1996, 69(3):371-373 . doi: https:// 10.1063/1.118064

[30] Hilfiker J N, Singh N, TIWALD T, et al. Survey of methods to characterize thin absorbing films with spectroscopic ellipsometry[J]. Thin Solid Films, 2008, 516(22):7979-7989. doi: https:// 10.1016/j.tsf.2008.04.060.

[31] Luangtip W, Rotbuathong S, Chindaudom P, et al. Investigation of Aluminium Diffusion into an Amorphous Silicon Thin Film at High Temperature by In Situ Spectroscopic Ellipsometry[J]. Advanced Materials Research, 2008, 55-57:449-452. doi: https:// 10.4028/www.scientific.net/AMR.55-57.449.

[32] J Koh, Y W Lu, C R Wronski, et al. Correlation of real time spectroellipsometry and atomic force microscopy measurements of surface roughness on amorphous semiconductor thin films[J]. Applied Physics Letters, 1996, 69(9):1297-1299. doi: https:// 10.1063/1.117397

[33] Katiyar P, Jin C, Narayan R J. Electrical properties of amorphous aluminum oxide thin films[J]. Acta Materialia, 2005, 53(9): 2617-2622. doi: https:// 10.1016/j.actamat.2005.02.027.

[34] Wei B, Chen H, Hua W, et al. Formation mechanism and photoelectric properties of Al_2O_3 film based on atomic layer deposition[J]. Applied Surface Science, 2022, 572: 151419. doi: https:// 10.1016/j.apsusc.2021.151419.

[35] Aarik L, Mandar H, Ritslaid P, et al. Low-temperature atomic layer deposition of α- Al_2O_3 thin films[J]. Crystal Growth & Design, 2021, 21(7): 4220-4229. doi: https:// 10.1021/acs.cgd.1c00471.

[36] Jinesh K B, Van Hemmen J L, Van De Sanden M C M, et al. Dielectric properties of thermal and plasma-assisted atomic layer deposited Al_2O_3 thin films[J]. Journal of The Electrochemical Society, 2010, 158(2): G21-G26. doi: https:// 10.1149/1.3517430.